

# Design of an electron microscope phase plate using a focused continuous-wave laser

H. Müller,<sup>1</sup> Jian Jin,<sup>2</sup> R. Danev,<sup>3</sup> J. Spence,<sup>4</sup> H. Padmore,<sup>5</sup> and R.M. Glaeser<sup>6</sup>

<sup>1</sup>*Physics Department, University of California, Berkeley, CA 94720\**

<sup>2</sup>*Engineering Division, Lawrence Berkeley National Laboratory, University of California, Berkeley, CA 94720*

<sup>3</sup>*Division of Nano-Structure Physiology, Okazaki Institute for Integrative Bioscience,*

*5-1 Higashiyama, Myodaiji, Okazaki 444-8787, Japan*

<sup>4</sup>*Physics Department, Arizona State University, Tempe, AZ 85287-1504*

<sup>5</sup>*Advanced Light Source, Lawrence Berkeley National Laboratory University of California, Berkeley, CA 94720*

<sup>6</sup>*Life Sciences Division, Lawrence Berkeley National Laboratory, University of California, Berkeley, CA 94720*

(Dated: October 30, 2018)

We propose a Zernike phase contrast electron microscope that uses an intense laser focus to convert a phase image into a visible image. We present the relativistic quantum theory of the phase shift caused by the laser-electron-interaction, study resonant cavities for enhancing the laser intensity, and discuss applications in biology, soft materials science, and atomic and molecular physics.

PACS numbers: 07.78.+s, 41.75.Ht, 42.60.Da, 87.64.mh

## I. INTRODUCTION

The resolution of modern transmission electron microscopes (TEMs) [1] can be more than 10,000 times the one of light microscopes. Yet, their imaging performance for thin soft matter such as biological specimens is limited: These specimens are weakly scattering phase objects and a perfect image of them shows almost no contrast. The image is imprinted, however, on the phase of the electron's wave function. In optical microscopes, such a phase image can be made visible by Zernike phase contrast microscopy [2]: the part of the light beam that has not been diffracted by the specimen is phase shifted by  $\pi/2$  by a quarter-wave plate, thus converting phase modulation into visible amplitude modulation.

Quarter-wave plates for TEMs have been suggested early [3] but could not be fabricated until recently. Examples are thin carbon film phase plates [4, 5], electrostatic (einzel lens) designs [6, 7], or thin bar magnets [8]. Although the most recent implementations are greatly improved over earlier versions [9], they are still prone to becoming electrostatically charged when they are hit by an electron beam. This causes distortion of the image. While it ought to be possible to overcome this limitation by using suitable materials and by keeping the surface of devices extremely clean, such solutions are not necessarily well suited for routine TEM applications. Moreover, microfabricated phase plates induce electron loss, leading to reduced performance.

Attempts have also been made to use bi-prism electron holography to record the phase of the electron beam, but this approach has been largely abandoned because subtle charging effects in the specimen itself result in degraded temporal coherence in an off-axis hologram, whereas they have little effect on the in-line holography that is provided by Zernike phase-contrast imaging.

In view of these challenges, the phase shift that occurs when an electron passes through a beam of light [10] is here envisioned as an alternative way to achieve phase contrast. To provide the high required laser intensities, a pulsed laser can be used together with a synchronized pulsed TEM [11]. However, using a pulsed-source TEM introduces new constraints for routine TEM applications, e.g., lower averaged electron flux and thus longer data collection periods, as the electron density during a pulse cannot be higher than in cw operation to avoid space charge effects, and potentially greater complexity.

In this Article, we propose designs for a continuous wave (cw) version of an optical-beam quarter-wave plate that we believe will be suitable for general use in a TEM. We will derive the phase shift of an electron wave and discuss implementations that reach the required small spot size and high intensity using focussing optics and optical cavities. Finally, we will discuss applications for biological specimens and other soft-matter specimens and give an outlook on other potential applications.

## II. ORIGIN OF THE PHASE SHIFT

The phase shift of the electron wave function caused by the laser can be explained by the ponderomotive force, a repulsive force felt by electrons entering the electric field of a laser. It is given by [12]  $\phi = \hbar\alpha\lambda\rho\delta t/m$ , where  $\hbar$  is the reduced Planck constant,  $\alpha$  the fine structure constant,  $\lambda$  the laser wavelength,  $\rho$  the photon density,  $m$  the electron mass, and  $\delta t$  the time interval. This is a nonrelativistic result. In the TEM, however, the electron energy is comparable to  $mc^2$  and thus relativistic corrections may be significant.

In order to obtain a relativistically correct result, we now derive the phase shift using the theory of quantum electrodynamics [13]. The electrons, long before the interaction with the laser, are described by a quantum state  $|i\rangle$ . A scattering matrix  $S = 1 + S^{(1)} + S^{(2)} + \dots$  describes the evolution of  $|i\rangle$  into the final state  $|f\rangle = S|i\rangle$ , which

\*Electronic address: hm@berkeley.edu

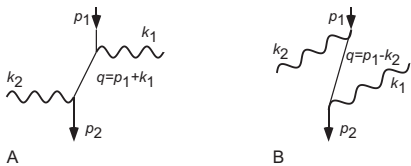


FIG. 1: Feynman diagrams for Compton scattering.  $p_1$ ,  $q$ , and  $p_2$  respectively denote the initial, intermediate, and final momentum of the electron,  $k_1$  and  $k_2$  are the photon momenta.

we define long after the interaction. The first order  $S^{(1)}$  describes emission or absorption of a single photon by an electron. This violates energy and momentum conservation, so  $S^{(1)} = 0$ . It is important for us that this still holds if the laser beam is focussed: the electric field of the focussed beam can be described in the momentum representation by a superposition of plane waves of various directions. Since  $S^{(1)} = 0$  for each of these plane waves, regardless of their direction or polarization, it is also zero for the focussed beam.

The leading nonzero effects are described by the second order,  $S^{(2)}$ . Most of these take place whether or not the electrons interact with the laser (*e.g.*, annihilation, electron-electron scattering, self-energy, and vacuum polarization [13]) and do not contribute to the phase shift of interest. The remaining process (Fig. 1), called Compton scattering, can transfer momentum and energy to the electron. The scattering rate for such transfer happens is  $r = \sigma_T \rho v$ , where  $\sigma_T = [\alpha \hbar / (m c^2)]^2$  is the Thomson cross section and  $v$  the electron velocity. Since electrons whose momentum has changed do not contribute to the TEM image, Compton scattering with momentum transfer is a loss mechanism.

The desired phase shift is caused by the degenerate case of Compton scattering without momentum transfer. From the Feynman diagrams in Fig. 1, the scattering matrix  $S$  can be calculated by following the Feynman rules, see Ref. [13], chapter 7.3. If we define  $\phi \equiv \langle f | S^{(2)} | i \rangle$ , the result can be expressed as (using  $\hbar = m = c = 1$ )

$$\begin{aligned} \phi &= \frac{(2\pi)^4 \delta^{(4)}(p_1 + k_1 - p_2 - k_2)}{2V^2 \sqrt{E_{p_1} E_{p_2} \omega_{k_1} \omega_{k_2}}} (S_A + S_B), \\ S_A &= -e^2 \bar{u}(\vec{p}_2) \not{\epsilon}(\vec{k}_2) i S_F(q) \not{\epsilon}(\vec{k}_1) u(\vec{p}_1) a^\dagger(\vec{k}_1) a(\vec{k}_2), \\ S_B &= -e^2 \bar{u}(\vec{p}_2) \not{\epsilon}(\vec{k}_1) i S_F(q) \not{\epsilon}(\vec{k}_2) u(\vec{p}_1) a^\dagger(\vec{k}_2) a(\vec{k}_1). \end{aligned} \quad (1)$$

$S_A$  and  $S_B$  denote terms arising from Fig. 1, A and B. Here,  $\delta^{(4)}$  is the four dimensional Dirac delta function,  $V$  the normalization volume,  $E_p$  the energy of an electron of 4-momentum  $p$ ,  $\omega_k$  the photon frequency,  $S_F$  the Feynman propagator [13], and  $u$  and  $\not{\epsilon}$  describe electron and photon polarization, respectively. Since no momentum is transferred,  $\vec{k}_1 = \vec{k}_2$  and we identify  $\rho \equiv a^\dagger(\vec{k}_1) a(\vec{k}_1) / V$  as the photon density operator. Physically, this means that the emission of the outgoing photon is stimulated by the laser, in contrast to the non-degenerate case that is treated in most textbooks. We obtain [14]  $\phi = -[i e^2 \rho / (2 E_p \omega)] \bar{u}(\vec{p}) [(\not{k}) / (pk)] u(\vec{p}) \delta t$ .

In our TEM (Fig. 3), the electron beam travels along the  $z$  axis and the laser orthogonally along  $y$ . Furthermore, we choose the polarization of the laser orthogonal to the direction of the electron beam. It follows that  $pk = -E_p \omega + \vec{p} \vec{k} = -E_p \omega$  and

$$\phi = \frac{-e^2 \rho \delta t}{2 E_p^2 \omega^2} \bar{u}(\vec{p}) [-\gamma^0 \omega + \gamma^2 k] u(\vec{p}) = \frac{\hbar \alpha \rho \lambda \delta t}{\sqrt{m^2 + p^2 / c^2}}. \quad (2)$$

This agrees with the non-relativistic result if  $p/c \ll m$ .

If the laser is polarized parallel to the electron beam,  $pk = -E_p \omega + p_z k_z$  and  $\phi = (1/2) \lambda \hbar \alpha \rho \delta t / (p_z / c - \sqrt{m^2 + p^2 / c^2})$ . For nonrelativistic electrons, this is a factor of two lower than Eq. (2).

We remark that we have treated the laser beam as a plane wave. A focussed beam could be described by a superposition of plane waves in the momentum representation. We can treat each of them in the above manner and calculate the combined effect. This will not lead to strong modifications of our results, because (i) even for the strongly focussed beams considered below, the major part of the optical power propagates at wavevectors having relatively small angles with the optical axis, and (ii) even for arbitrary wavevectors, the phase shift caused is not zero or of opposite sign, ruling out cancellations.

If  $\phi \ll 1$ , it clearly describes a phase shift:  $|f\rangle = (1 + i\phi) |i\rangle \approx e^{i\phi} |i\rangle$ . To see that this still holds for large  $\phi$ , we divide the time interval  $\delta t$  into several small ones. Repeated application of the  $S^{(2)}$ , once for each small interval, shows that  $|f\rangle = e^{i\phi} |i\rangle$ . This process amounts to summing an infinite series of Feynman diagrams, in which the processes of Fig. 1 A, B happen 1,2,3,... times. This is valid as long as other processes such as non-degenerate Compton effect remain negligible. This is satisfied in our case: the fraction of electrons lost per radian of phase shift is given by  $r/\phi = \alpha(v/c)(\lambda_C/\lambda)$ . This is about  $10^{-8}$  for  $\lambda = 1 \mu\text{m}$  and thus negligible.

### III. DESIGN OF THE LASER PHASE PLATE

#### A. Near-spherical cavity

We now study how this phase shift can be applied for a cw phase contrast TEM. The basic challenge is to reach a sufficient photon density, which requires a large laser intensity. However, since the phase shift is proportional to the laser wavelength  $\lambda$ , we can use the longest wavelength at which we can still achieve a focus of the required size. The smallest focus for a given wavelength is achieved by the  $\text{TM}_{n01}$  mode in a spherical resonant cavity [17] shown in Fig. 2 B. The cavity provides both focussing as well as resonant enhancement of the intensity: the laser has to supply only the power lost at the cavity walls. The focus has a half-intensity radii of  $0.25\lambda$  and  $0.20\lambda$  in  $x$  and  $y$ -direction, respectively; the largest intensity maxima other than the focus are less than 10% of the intensity at the focus and can be neglected.

To determine the required laser power, we calculate the energy flow  $3E_0^2\pi/(4c\mu_0k^2)$  towards the cavity walls, where  $E_0$  is the peak electric field at the focus, given the electric field in the cavity [17]. The cavity walls reflect most of this back, but  $P = 3(1-r)E_0^2\pi/(4\eta k^2)$ , where  $r$  is the reflectivity of the cavity walls is lost and has to be replaced by the laser. Expressing the photon density by the electric field  $E_z^2 = 2\rho\hbar\omega c\mu_0$  (where the factor of 2 accounts for the time averaging of the intensity) and integrating along the  $z$ -axis  $\int_{-\infty}^{\infty} E_z^2(x=0, y=0, z)dz = \frac{3}{5}E_0^2\lambda$ , we obtain  $\phi = \frac{4}{5(1-r)}\frac{\lambda P\alpha}{\gamma c^2 m v}$ , where  $\gamma = 1/\sqrt{1-v^2/c^2}$ , or

$$\frac{\delta}{\pi/2} \approx \gamma^{-1} \left( \frac{P}{\text{kW}} \right) \left( \frac{\lambda}{\mu\text{m}} \right) \left( \frac{v}{c} \right)^{-1} \mathcal{N}, \quad (3)$$

where  $\mathcal{N} \approx 0.15/(1-r)$ .

Such cavities can use metal coatings for the inner walls. For gold, for example,  $r \approx 0.98$  in the infrared. Achieving optimal phase contrast with a cut-on spatial frequency of  $1/(40 \text{ nm})$  with a modified FEI Titan electron microscope that is available at Berkeley requires a half-intensity radius of about 2 microns at an electron energy of 80 keV or 1 micron at 300 keV. The longest wavelength at which a  $2\mu\text{m}$  focus can be achieved is about  $\lambda \sim 10\mu\text{m}$ . If we choose a  $\text{CO}_2$  laser at  $10.6\mu\text{m}$  and let  $r = 0.98$  and  $v = c/2$ , we need a power of about 7.5 W. A 1-micron focus can be achieved using  $P = 39 \text{ W}$  at  $\lambda = 2 \text{ m}\mu\text{m}$  or  $P = 75 \text{ W}$  at 1064 nm.

To help coupling the laser power into the  $\text{TM}_{n01}$  mode, distortion of the sphere will lift the degeneracy of modes: the desired mode can then be selected by tuning the laser frequency. Coupling the laser beam into the cavity can be achieved, *e.g.*, via a hole of radius  $r_{\text{in}} = R\sqrt{2(1-r)}/3$  in the cavity, where  $R$  is the radius of the cavity. This radius is determined such that the power lost at the walls balances the one delivered through the hole when the electromagnetic field of the laser matches the resonant field inside the sphere. The laser-cavity coupling efficiency is then given by the overlap integral of the laser and the cavity field. For a Gaussian laser beam, the optimum power transfer is 50.4% and occurs when the  $1/e^2$  intensity radius ('waist') of that beam equals the hole radius and a lens of appropriate focal length is used (Fig. 2 A). The overlap can be increased by transforming the Gaussian beam into a uniform-intensity beam, which is possible with 84-90% efficiency [18, 19]. In order to maintain resonance, the laser frequency can be stabilized to the cavity resonance (or vice versa) using the Pound-Drever-Hall [20] or similar methods.

### B. Plano-parabolic cavity

A parabolic mirror with radius much larger than focal length produces a focus with an electric field similar to the one in a spherical cavity. Together with a planar partial mirror, a plano-parabolic cavity can be realized,

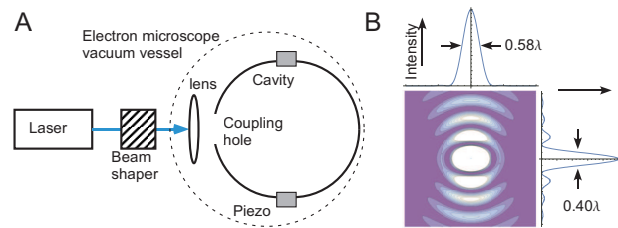


FIG. 2: A: setup for a phase contrast TEM using a near-spherical resonant cavity. The electron beam is propagating orthogonal to the paper plane. B: Intensity of the  $\text{TM}_{n01}$  mode in a spherical cavity. Shown is a 2-dimensional contour plot as well as the intensities along the  $x$  and  $y$  axes through the focus, respectively.

see Fig. 3. This is easier to manufacture, as no hollow spheres need to be produced. Moreover, the partial mirror is planar or near-planar and can thus have a low-loss dielectric coating. Finally, the laser beam feeding the cavity is collimated, simplifying mode-match. The phase shift is given approximately by the same equation as for the sphere, but  $r$  is replaced by an effective reflectivity  $r_{\text{eff}}$ , which is reduced because of losses when the photons spill over the perimeter of the mirror.  $r_{\text{eff}} = 0.9$  might be possible, and the required laser power is now 35 W. Such an arrangement could thus satisfy all requirements using a  $\text{CO}_2$  laser.

### C. Fabry-Perot cavity

Power buildup by factors of 100,000 or more [21] are possible with high-reflectivity dielectric mirrors. Unfortunately, they can at present only be applied to relatively flat surfaces. Cavities using such mirrors are called Fabry-Perot cavities; their eigenmodes are Gaussian beams [15]. In order to keep losses due to the mirror aperture below a part per million, we choose the mirror radius  $r_m \gtrsim (5/2)w(L/2)$ , where  $w(L/2)$  is the  $1/e^2$  intensity radius of the beam at the mirrors. This results in a radius  $w_0 = (5/2)\lambda/(\pi\text{NA})$  of the focus, where  $\text{NA} = r_m/R$ . The phase shift is given by Eq. (3) where the factor  $\mathcal{N} = 0.030/(1-r)$ .

At present, commercial dielectric mirrors reach  $\text{NA}=0.04$ . At  $\lambda = 532 \text{ nm}$  and a Finesse  $\mathcal{F} \equiv \pi/(1-r) = 50,000$ , we would thus need a laser power of 8 W, which is available from commercial lasers. However, to obtain an  $1/2$  intensity radius of  $2\mu\text{m}$ , which corresponds to an  $1/e^2$  intensity radius of  $w_0 = 1.7\mu\text{m}$ , a minimum  $\text{NA}=0.25$  is required at  $\lambda = 532 \text{ nm}$ . If such a cavity could be built with a Finesse of 7,500, it would reach the required phase shift with an 8 W laser. Even then, however, the standing wave in the cavity will have a large number of maxima and minima along the beam direction, forming a phase grating that diffracts the electron beam and is thus undesirable. Also, the half width of the intensity in the  $y$  direction is given by the Rayleigh range

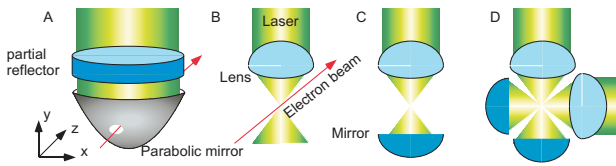


FIG. 3: Alternative realizations of laser phase plates. A: plano-parabolic cavity; B: high-NA lens; C: high-NA lens with retroreflector; D: two focused, retroreflected beams. The electron beam is propagating orthogonally to the page.

$z_R \approx \pi\lambda/(2NA)^2$ , and is even larger than  $w_0$ . These disadvantages are alleviated at high  $NA \approx 1$ , which makes the central maximum dominate.

#### D. Designs without cavity

A simple way to achieve this is a lens of large numerical aperture NA, see Fig. 3, not using a cavity. If the aperture of the lens is  $3/2$  times the waist  $w(f)$  at the lens (so that it transmits 99% of the laser power) the resulting radius of focus is  $w_0 \approx \lambda/(2NA)$ . The phase shift is given by Eq. (3) with  $\mathcal{N} = 0.048NA$ . With a NA of 1, the maximum wavelength in this implementation is about  $3 \mu\text{m}$ . Unfortunately, a power of about 4 kW would be required even if  $NA=1$ . At  $\lambda = 10.6 \mu\text{m}$  with  $NA=1$ , this is reduced to  $P = 1.2 \text{ kW}$  is required, but this results in  $w_0 = 5 \mu\text{m}$ , about 3 times too large.

In Fig. 3 C, a standing wave is generated, which has a half-intensity half-width of  $\lambda/8$  in the beam direction at the cost of a more complicated intensity profile that has several minor peaks. If the focal point of the lens and the mirror coincide, the electric field there is doubled and the intensity quadrupled, resulting in  $\mathcal{N} = 0.19NA$ . To obtain low spot size in two dimensions, two standing waves can be overlapped as shown in Fig. 3, D. If these two beams have polarizations orthogonal to the electron beam, and thus orthogonal to each other, their electric fields add geometrically and  $\mathcal{N} = 0.19NA$ . A similar implementation might use the focused spot as in Fig. 3 B and use mirrors to turn the beam 270 degrees and bring it in through a second lens, similar to Fig. 3 D. We remark that at high NA, the theory of Gaussian beams becomes inaccurate [16]. Depending on the combination of optics and polarization, a factor of safety of 1.2-2 should be applied to the above estimates at  $NA=1$ . This is a further advantage of the spherical or plano-parabolic cavity, where exact analytical expressions have been used to calculate the fields.

#### IV. APPLICATIONS

At present, the spherical or plano-parabolic cavities appear to be the most promising approaches to construct a cw laser phase plate. Such a phase plate has a num-

ber of important advantages over microfabricated ones: Since it does not use mechanical structures inside or near the electron beam, it can be completely free of the unwanted electrostatic charging that can occur when electrons hit a solid-phase target, under conventional vacuum conditions. Also, almost none of the electrons that pass through the optical beam are lost, in contrast to thin film or microfabricated phase plates. Moreover, laser phase plates are not subject to the aging experienced by thin carbon-film phase plates [22].

Development of such a reliable phase plate would significantly expand the usefulness of TEMs in biology and in soft-materials science. In current practice, the only option for generating contrast for thin organic materials like biological specimens is to emulate a phase plate by intentionally using a rather large amount of defocus, combined with spherical aberration [23]. Contrast transfer in a defocused TEM image is quite poor, for example, for the low spatial frequencies that carry most of the information about the size, shape, and location of an object; it also suffers from contrast reversals (and accompanying zeros) as well as from a damped envelope at higher resolution, when the amount of defocus is increased enough to improve the contrast transfer at low frequencies. By contrast, the laser phase plate would provide full image contrast at low and high resolution at the same time. Use of a quarter-wave phase plate in biology will make it possible to image much smaller protein complexes than can currently be visualized by defocus-based phase contrast, as has been demonstrated with the use of a thin-film phase plate [22]. In most soft-matter applications, the density differences are even smaller than they are for biological materials that are embedded in vitreous ice, and thus it is hardly possible to image polymer blends, etc. with defocus-based phase contrast. In soft-matter applications, the use of a quarter-wave phase plate will thus open up greater possibilities for imaging unstained specimens under low-dose conditions.

#### V. OUTLOOK

As an outlook, the intense 3 dimensional laser foci generated for this work can also be used as very deep dipole traps for electrons [25], atoms, and molecules. Trap depths could be in the range of tens or even hundreds of Kelvin, allowing, for example, to trap room-temperature atoms of almost any kind and localize them to better than 0.5 microns. This would allow for spectroscopy of exotic species. For example, spectroscopy of the  $\sim 5\text{-}6 \text{ eV}$  transition in the Thorium 229 nucleus would allow for the construction of clocks based on nuclear energy levels but has so far been thwarted by the lack of a suitable atom trap. The dipole trap proposed here could solve this problem and thus lead to higher precision clocks (as the nucleus of an atom is less sensitive to the environment than the electron shell), tests of the time variability of fundamental constants of unprecedented accuracy, or searches for an

electron electric dipole moment [24]. Moreover, a phase contrast TEM could be used for scattering-free quantum nondemolition imaging of atoms, ions, or molecules.

### Acknowledgments

We thank Eva Nogales for discussions and Mike Hohensee for help in preparing the manuscript. This re-

search was supported by NIH grant GM083039, the David and Lucile Packard Foundation, and the Alfred P. Sloan foundation.

- 
- [1] R. Glaeser, K. Downing, D. DeRosier, W. Chiu, and J. Frank, *Electron Crystallography of Biological Macromolecules* (Oxford University Press, 2007); J.C.H. Spence. *High resolution electron microscopy*. (Oxford University Press, New York 2003).
- [2] F. Zernicke, *Physica* **9**, 686-698, (1942); *ibid.* 974-986 (1942); *Science* **121**, 345-349 (1955).
- [3] H. Boersch, *Z. Naturforsch.* 2A (1947) 615.
- [4] F. Hosokawa, R. Danev, Y. Arai, and K. Nagayama, *J. Electron Microscopy* **54**, 317-324 (2005).
- [5] K. Nagayama and R. Danev, *Philos. Trans. R. Soc. London B* **363**, 2153-2162 (2008).
- [6] K. Schultheiß, F. Pérez-Willard, B. Barton, D. Gerthsen, and R.R. Schröder, *Rev. Sci. Instr.* **77**, 033701 (2006).
- [7] R. Cambie *et al.*, *Ultramicroscopy* **107**, 329-339 (2007).
- [8] K. Nagayama and R. Danev, *Biophys. Rev.* **1**, 3742 (2009).
- [9] R. Danev and K. Nagayama, *Ultramicroscopy* **88**, 243-252 (2001).
- [10] D.M. Volkov, *Z. Physik* **94**, 250 (1936); J. F. Dawson and Z. Fried, *Phys. Rev. Lett.* **19**, 467 (1967); V. Berestekskii, E. M. Lifshitz and L.P. Pitaevskii, *Relativistic Quantum Theory* (Pergamon Press, 1971) p.122).
- [11] [https://ipo.llnl.gov/?q=technologies-phase\\_plate](https://ipo.llnl.gov/?q=technologies-phase_plate)
- [12] B. Barwick and H. Batelaan, *New J. Phys.* **10**, 083036 (2008).
- [13] F. Mandl and G. Shaw, *Quantum Field Theory* (Wiley, 1993), in particular sections 6 and 7.
- [14] We used  $(\vec{p} + \vec{k})^2 - 1 = 2pk$ ,  $\not{\epsilon} = \epsilon^2 = 1$ , and  $(2\pi)^4 \delta^{(4)}(0) \rightarrow V\delta t$  [13].
- [15] A.E. Siegman, *Lasers* (University Science Books, Sausalito 1986).
- [16] M.A. Lieb and A.J. Meixner, *Optics Express* **8**, 458-474 (2001); J. Lekner, *J. Opt. A* **5**, 614 (2003); K. Lindfors *et al.*, *Nature Photonics* **1**, 228 (2007).
- [17] K. Zhang, and D. Li, *Electromagnetic Theory for Microwaves and Optoelectronics* (Springer, Berlin, 2007).
- [18] Y. Matizen and Y.V. Troitskii, *Sov. J. Quantum Electron.* **19**, 398-402 (1989).
- [19] D. Palima and J. Glückstad, *Opt. Express*, **16**, 1507-1516 (2008).
- [20] R.W.P. Drever *et al.*, *Appl. Phys. B*, 31, 97105 (1983).
- [21] C.J. Hood, H.J. Kimble, and J. Ye, *Phys. Rev. A* **64**, 033804 (2001).
- [22] R. Danev, R.M. Glaser, and K. Nagayama, *Ultramicroscopy* **109**, 312-325 (2009).
- [23] M. Lentzen, *Ultramicroscopy* **99**, 211220 (2004).
- [24] *Lepton Dipole Moments*, ed. B.L. Roberts and W.J. Marciano, World Scientific (2009).
- [25] C.I. Moore, *J. Mod. Optics*, **39** 2171 (1992).